Title: Characterization of Structural and Electronic Transitions During Reduction and Oxidation of Ruthenium Acetylacetonate Flow Battery Electrolytes Using X-Ray Absorption Spectroscopy

Authors: Jonathan Kucharyson; Jason Gaudet; Brian Wyvratt; Levi Thompson

To be cited as: ChemElectroChem 10.1002/celc.201600360

Link to VoR: http://dx.doi.org/10.1002/celc.201600360

WILEY-VCH

DOI: 10.1002/ ((please add manuscript number))

Article type: Full Paper

Characterization of Structural and Electronic Transitions During Reduction and Oxidation of Ruthenium(III) Acetylacetonate-Based Flow Battery Electrolytes Using X-Ray Absorption Spectroscopy

*Jonathan F. Kucharyson, Jason R. Gaudet, Brian M. Wyvratt and Levi T. Thompson**

J.F. Kucharyson, J.R. Gaudet, B.M. Wyvratt, Prof. L.T. Thompson

University of Michigan – Phoenix Memorial Lab, 2301 Bonisteel Blvd, Ann Arbor, MI 48109, United States of America

E-mail: ltt@umich.edu

Keywords: Redox flow batteries, X-ray absorption spectroscopy, Acetylacetonates, Energy-storage

Abstract

Metal acetylacetonates possess several very attractive electrochemical properties, however, their cyclabilities fall short of targets for use in non-aqueous redox flow batteries. This paper

describes structural and compositional changes during the reduction and oxidation of ruthenium(III) acetylacetonate ($Ru(acac)_3$), a representative acetylacetonate. Voltammetry, bulk electrolysis and *in situ* X-ray absorption spectroscopy (XAS) results are complemented by those from density functional theory (DFT) calculations. The reduction of $Ru(acac)_3$ in acetonitrile is highly reversible, producing a couple at -1.1 V vs. Ag/Ag^+. *In situ* XAS and DFT indicates the formation of $[Ru(acac)_3]^-$ with Ru-O bonds lengthened relative to $Ru(acac)_3$, nearly all of the charge localized on Ru, and no ligand shedding. The oxidation of $Ru(acac)_3$ is quasi-reversible with a couple at 0.7 V. The initial product is likely $[Ru(acac)_3]^+$, however, this species is short-lived, converting to a product with a couple at -0.2 V, structure that is nearly identical to that of $Ru(acac)_3$ within 3 Å of Ru, and ~70% of the charge extracted from Ru (balance from acetylacetone). This non-innocence likely contributed to the instability of $[Ru(acac)_3]^+$. Taken together, the results suggest that the stabilities and cyclabilities of acetylacetonates are determined by the degree of charge transfer to/from the metal.

1. Introduction

One of the major hurdles facing the integration of electricity derived from renewable resources into the grid is their temporal variability.[1] As a result, significant emphasis has been placed on the development of large-scale energy storage devices. In addition to allowing for the controlled distribution of renewable energy,[2] large-scale energy storage could enable higher efficiencies for existing energy generation technologies.[3]

While a number of energy storage technologies are being investigated[4], redox flow batteries (RFBs) have been demonstrated to have a unique combination of attractive characteristics including long lifetimes due to their decoupled power and energy, and the potential to reach high energy densities.[5] RFBs consist of solvated active species (electrolytes) which are stored in reservoirs to prevent self-discharge.[5] These electrolytes are pumped past electrodes that are separated by a membrane. During charging, one of the electrolytes (catholyte) is

oxidized and the other (anolyte) is reduced. The reverse occurs during discharge. For the purposes of clarity in this paper, the catholyte (oxidation) reaction will be referred to as the positive couple, and the anolyte (reduction) reaction will be referred to as the negative couple. All commercially available RFBs are based on aqueous electrolytes, and while they have been demonstrated to have high cycle lives,[5] the electrochemical window of water (1.23V)[6] results in relatively low energy densities and high cost. Darling and coworkers indicate that an active species of sufficiently low molecular weight and high cell potential, could enable non-aqueous RFBs that meet the aggressive Department of Energy goal of $100 per kWh.[7] Many non-aqueous solvents including acetonitrile allow for much higher potentials than water, in some cases as high as 5V.[6]

A variety of metallo-organic[8–28] and organic complexes[29–33] have been investigated for use as active species in non-aqueous RFB electrolytes. Metal acetylacetonates such as $V(acac)_3$ and $Cr(acac)_3$ are particularly attractive as they are capable of multielectron transfers, in some cases with redox couples that are separated by more than 2V[20,22,24], and their solubilities can be manipulated over more than 4 orders of magnitude via functionalization of the acetylacetone backbone.[26] Cycling solutions of metal acetylacetonates in acetonitrile reveals significant capacity fade that is often attributed to irreversible ligand shedding and/or irreversible oxidation reactions.[17–19,21,26] Chromium(III) bipyridine complexes have six redox couples over a ~2V window and solubilities approaching 1M.[10] The multielectron transfer capabilities have been linked to non-innocence (redox activity) of the bipyridine ligands. When cycled in an H-cell, however, solutions of $Cr(bpy)_3$ in acetonitrile reach less than 30% of their theoretical capacities, and significant capacity fade occurs.[10] Wei and co-workers were able to cycle a ferrocenium complex $[Fe(C_5H_5)_2CH_2N(CH_3)_2CH_2CH_3]\ N(SO_2CF_3)_2$ in a flow cell for 100 cycles with 95% capacity retention at 0.1M. When cycled at 0.8M

concentrations, however, significant capacity fade occurred during the first 20 cycles.[34] The same group recently reported reduced capacity fade for the same complex at 1.2M for 500 cycles in a static cell.[16] The cause of the fade, in most cases, has not been investigated and consequently is not well understood. While cyclic voltammetry (CV) of these metallo-organic and organic complexes often demonstrate promising fundamental attributes, none possess sufficient cycle lives, in particular at the high concentrations needed for commercial applications.

Research described in this paper used *in situ* x-ray absorption spectroscopy (XAS) to investigate the cause of instabilities for metal acetylacetonate based electrolytes. XAS is one of the more powerful techniques for characterizing the electronic and physical structures of materials under *in situ* conditions. This technique utilizes high energy x-rays that can be tuned to excite core electrons of a selected element. The resulting spectra consists of two regions: the x-ray absorption near-edge structure (XANES), which can be used to quantify the oxidation state of the element being investigated, and the extended x-ray absorption fine structure (EXAFS), which can be used to determine structural details. Apblett and co-workers recently reported the use of XAS to monitor the oxidation state and structural changes of an Fe-based ionic liquid ($Fe((OHCH_2CH_2)_2NH)_6$-$(CF_3SO_3)_3$). Partial charging was observed but the exact oxidation state changes were not determined due to mixing issues within the cell. They also reported that the Fe-O bonds were lengthened during oxidation, as expected based on the anionic oxygens, but no bond lengths changes were detected during reduction. It is possible that side reactions occurred as the electrolyte and cell were prepared while in contact with air.[35] To our knowledge this is the only report of the use of XAS to characterize a non-aqueous RFB electrolyte.

While the cost and limited solubility of ruthenium(III) acetylacetonate ($Ru(acac)_3$) prevent it from being utilized as a commercial RFB active material, it does represent an interesting case study for understanding how the structures and charge distributions are affected by electrochemical oxidation and reduction. Due to the weak x-ray absorption of acetonitrile at the Ru K edge (22 keV), transmission measurements through a functioning cell can probe the Ru without excessive signal loss due to matrix absorption. $Ru(acac)_3$ was also selected because its properties are similar to those of the other metal acetylacetonates and the cause for fade is unknown. Chakbarati and co-workers reported that while $Ru(acac)_3$ undergoes two quasi-reversible redox reactions over a 2V window in acetonitrile, less than 12% state of charge (SOC) was achieved during charge/discharge experiments.[27] This suggests that products formed during CV were different from those formed during charge/discharge experiments or that the initial products converted to other species. *In situ* XAS will allow us to characterize these species. The XAS was performed in specially designed electrochemical cells that allowed us to track changes in the structural and electronic properties of solvated $Ru(acac)_3$ while the material was being electrochemically oxidized or reduced, and isolated from air.

Our experimental protocol started by using CV to determine the voltage ranges to be used during oxidation and reduction of the $Ru(acac)_3$ electrolytes. We then used bulk electrolysis (BE) to change oxidation states of the electrolytes. During BE, the electrolyte was held at a constant potential until a given degree of oxidation or reduction (i.e. SOC) was achieved or until the current decayed to essentially zero. When possible, the BE was carried out in steps of 0.2 electrons per molecule. The resulting materials were characterized using CV and XAS. In attempts to completely reduce $Ru(acac)_3$, the electrolyte was held at -1.5V; subsequently it was held at -0.7V to fully reoxidize the electrolyte. In attempts to completely oxidize

$Ru(acac)_3$, the electrolyte was held at 0.8V; subsequently it was held at 0.4V to reduce the electrolyte. The *in situ* XAS was performed in an air-tight teflon BE cell with windows to allow the x-ray beam to travel through the electrolyte. The experimental results were complemented by DFT structure optimization calculations using Gaussian 09, with Multiwfn for orbital density quantification.[36,37] Together the results allowed us to define the structural and compositional properties of the electrolyte and determine the cause for degradation of the $Ru(acac)_3$ based electrolytes.

2. Results and Discussion

2.1. Cyclic Voltammetry and Standard Potentials

The cyclic voltammogram of $Ru(acac)_3$ in acetonitrile is illustrated in Figure 1. Voltammograms of $Ru(acac)_3$ solutions have been previously reported to include two quasi-reversible couples separated by ~1.77V,[27] and as seen in Table 1, we observed similar results. Furthermore, the standard potentials generated by DFT are consistent with the experimental results. Figure 1 also reveals a minor couple at -0.2V vs. Ag/Ag^+ that was not previously reported. The origin of this feature will be discussed later.

The diffusion coefficient for $Ru(acac)_3$ in acetonitrile was determined using the Randles-Sevcik equation[20,22,24,26] and the results are listed in Table 1 (see Supplementary Information Figures S1-S3 for scan rate plots). This diffusion coefficient was within error of that for other acetylacetonate complexes[26], which is not unexpected given their structural similarities. While CV provides useful information regarding the short-term products of redox reactions, BE allows for the characterization of longer-term species that are more relevant to battery operation.

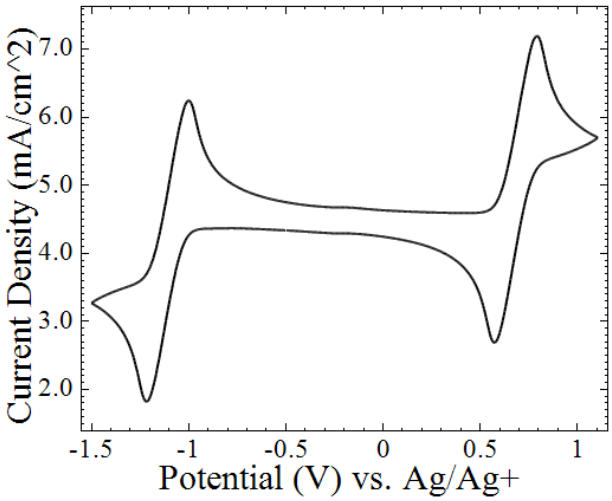

Figure 1. Cyclic voltammogram of 0.01M $Ru(acac)_3$ in acetonitrile with 0.1M $TBABF_4$.

Table 1. Standard potentials (E_0) and diffusion coefficients (D_0) determined by CV and DFT calculations. The standard potentials in V vs. Ag/Ag^+.

	E_0, Negative Couple [V]		E_0, Positive Couple [V]		D_0 [10^6 cm^2 s^{-1}]
	CV	DFT	CV	DFT	CV
$Ru(acac)_3$	-1.11	-1.09±0.02	0.68	0.73±0.09	6.1±0.8

2.2. Structural Changes During Reduction and Oxidization

During BE to completely reduce the $Ru(acac)_3$ solution, 0.95 electrons per molecule could be charged to the cell before the current decayed to zero, and 0.89 electrons per molecule could be extracted during the subsequent oxidation (see Supplementary Information Figure S4). The small difference in the number of electrons is primarily due to cross-over, as CVs before and after BE were similar (Figure 2). Based on the literature[27], the reaction associated with the couple at -1.1V is:

$$[Ru(acac)_3] + e^- \leftrightarrow [Ru(acac)_3]^- \quad (1)$$

The results suggest that $[Ru(acac)_3]^-$ is not subject to further changes with time (i.e. it has a long shelf life). Also note that the couple at -0.2V remains a very minor feature in the CV and is inactive at the potentials used for BE.

During BE to completely oxidize the $Ru(acac)_3$ solution, 1.11 electrons per molecule could be extracted from the cell before the current decayed to zero, but only 0.08 electrons per molecule could be charged to the cell during the subsequent reduction. The resting potential shifted from 0.7V to -0.2V. In fact the dominant couple in the CV after BE (Figure 2) is at -0.2V; consequently BE at 0.4 and 0.7V would have little effect on the electrolyte. The principal reaction associated with the couple at 0.7V has been reported to be:[27]

$$[Ru(acac)_3] \leftrightarrow [Ru(acac)_3]^+ + e^- \quad (2)$$

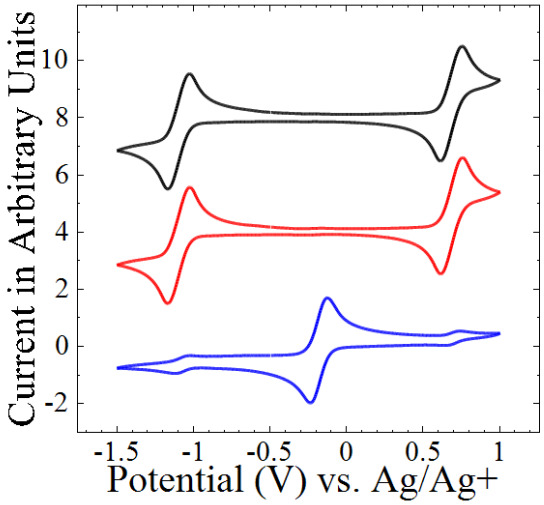

Figure 2. CV of $Ru(acac)_3$ electrolyte before (black), after reduction then oxidation (-1.5V then -0.7V) (red) and oxidation then reduction (0.8V then 0.4V) (blue).

While the short-term product could be $[Ru(acac)_3]^+$ based on the CV, results from BE suggest a different long-term product that yields a redox couple at -0.2V. This product is not free ligand, as the oxidation of acetylacetone is irreversible, occurring at ~0V vs Ag/Ag^+.[38] The peak height of the product suggests a diffusion coefficient that is comparable to that for $Ru(acac)_3$ in acetonitrile and, based on the Stokes-Einstein equation[39], this species is similar in size to $Ru(acac)_3$. The reversibility of the species giving rise to the couple at -0.2V was characterized by reducing the electrolyte at -0.5V, and subsequently oxidizing it at 0.4V. The BE of this species was very irreversible. The emergence of this species would explain the

difficulties reported previously in attempts to completely discharge cells employing $Ru(acac)_3$.[27]

EXAFS spectra of the electrolytes before and after BE are shown in Figure 3, along with illustrations of the relevant photoelectron paths. Each peak represents a half-path: the distance a photoelectron travels from the Ru atom to one or more scattering electrons and then back to the same Ru atom, divided by two by convention. For single-scatterer paths, this is simply the distance from the Ru atom to the scattering atom, while for two-scatterer paths this is half the perimeter of the triangle formed by the scatterers and Ru. The peak at 1.6Å corresponds to the ~2Å path of a photoelectron to the 6-fold oxygen nearest neighbor (R1). The peak at 2.5 Å corresponds primarily to the path of a photoelectron to the ~3Å 6-fold carbon second-nearest-neighbor (R2), overlaid with the triangular half-path from the Ru and around these same O and C atoms (R3, where the perimeter of this Ru-O-C triangle is 2R3). Using FEFF, these three paths were generated from a DFT-optimized $Ru(acac)_3$ and fit to the experimental data. Before BE, the Ru-O bond distance (R1), the second-nearest-neighbor Ru-C distance (R2) and the Ru-O-C triangle (2R3) were found to be 2.02±0.01Å, 2.94±0.02Å, and 6.2±0.1Å, respectively (see Supplementary Information Table S3). These distances indicate an O-Ru-C angle of 14°. The amplitude of this fit (where 1 represents $Ru(acac)_3$ and 0 represents a Ru atom with no local structure) was 1.0±0.1 and the variance of these bond distances was found to be σ^2 = 0.003±0.001Å, which is the expected value at room temperature; these values held during the entire course of experiments.

The electrochemical reduction of $Ru(acac)_3$ causes the Ru-O bond (R1) to lengthen from 2.02 to 2.05Å; subsequent oxidation causes the bond length to retract to its initial value (Figure 4). The average bond length varied linearly with the charge added or extracted per molecule. Although we expect these distances to represent two unique species - $Ru(acac)_3$ and

$Ru(acac)_3^-$ - the change in bond distances between them was too small to deconvolute into separate paths. Instead the bond length was taken as an average for these species. Variations in the bond length determined using EXAFS were consistent with those calculated by DFT (Table 2). The optimized structure, XYZ coordinates and bond length changes can be found in the Supplementary Information Figure S5 and Tables S1 and S2. The acetylacetonate ligand is negatively charged, and as the complex is reduced, the Ru-O bond should lengthen due to repulsive forces; the opposite should occur with an increasing oxidation state. Interestingly variations in R2 and R3 path distances were less than the estimated uncertainties, indicating minor changes in the corresponding bond lengths if any. The uncertainties for R2 and R3 are 0.02 and 0.05Å, respectively, so the photoelectron path length is likely changing, but within error. Alternatively, the ligand is distorted to allow for a slight increase in R1, without changing R2 or R3. The full set of EXAFS data are provided in the Supplementary Information (Table S3) along with a representative fit (Figure S6). Recall that there were minimal changes in the electrochemistry observed from CVs collected before and after BE to reduce $Ru(acac)_3$ (Figure 2). The reversible Ru-O bond changes are consistent with those findings.

When $Ru(acac)_3$ was electrochemically oxidized, the Ru-O bond length (Figure 4) decreased by less than 0.01Å; the small change was linear with the charge extracted. As was found during the reduction of $Ru(acac)_3$, the amplitude of the EXAFS paths does not deviate from 1.0±0.1; ligand shedding, if any, was less than 10%. This result is apparently inconsistent with the CVs which indicated significant changes in the electrochemistry (Figure 2) and presumably the structure of $Ru(acac)_3$ on oxidation. Based on the DFT calculations, a bond length change of 0.04Å should occur when $Ru(acac)_3$ is oxidized to $[Ru(acac)_3]^+$, providing further evidence for a species other than $[Ru(acac)_3]^+$. The EXAFS spectra allowed us to rule

out the formation of RuO_2 (1.9Å Ru-O bond), a Ru acetylacetonate dimer (2.6 Å Ru-Ru bond) or Ru metal (2.5 Å Ru-Ru bond) as products.[40] As our EXAFS measurements in the 3-6 Å range do not include enough data to deconvolute the large number of overlapping photoelectron paths generated by the acetylacetone ligand, we do not expect to observe any changes on the ligand 3Å from the Ru atoms. We have tentatively concluded that the structural and compositional changes occurred on the acetylacetone ligand, beyond the sampling range of EXAFS. The changes were irreversible and the resulting complex produces a couple at -0.2V vs Ag/Ag^+. The Ru XANES will provide important information regarding relative contributions of the Ru and the ligand to the electrochemistry. Nevertheless, additional characterization will be required to provide a highly detailed description of the species.

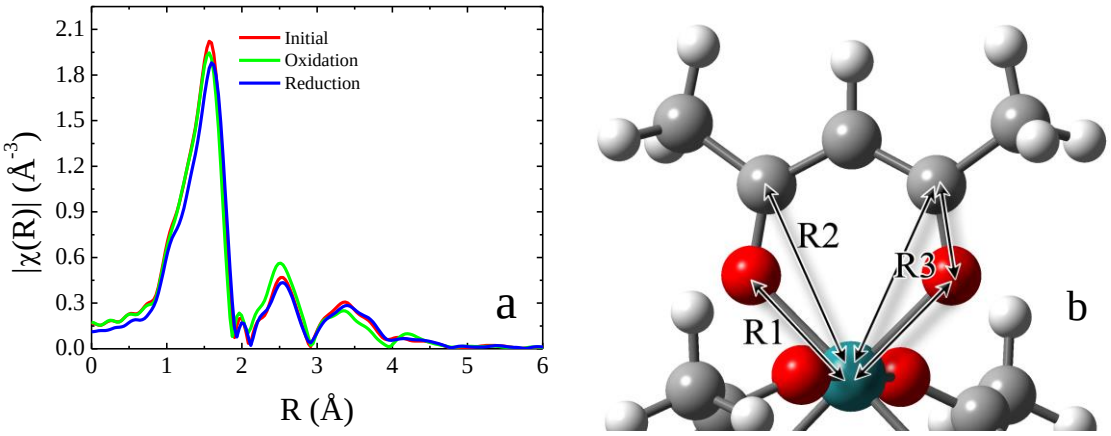

Figure 3. R-space EXAFS of $Ru(acac)_3$ before BE and following reduction and oxidation (k-weight=2) (a). Peaks at 1.6 and 2.5 are primarily formed from illustrated photoelectric paths (b). The peak at 3.3Å consists of a large number of ligand paths which could not be deconvoluted.

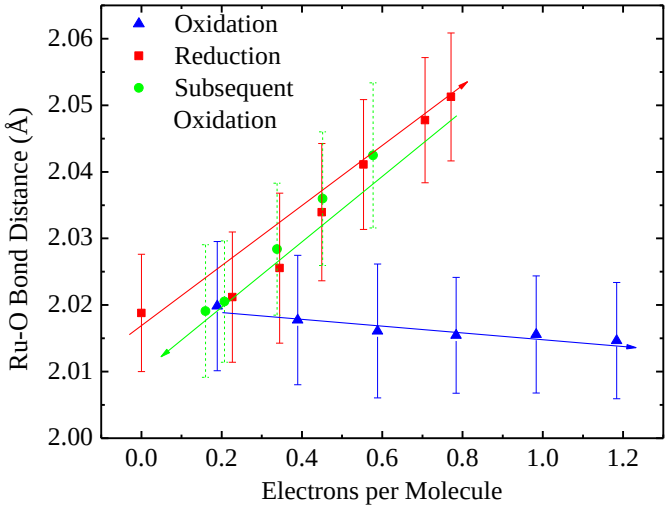

Figure 4. Changes in Ru-O bond length (Ru-O first shell) for $Ru(acac)_3$ during BE as determined using *in situ* EXAFS.

Table 2. Measured (EXAFS) and computed (DFT) bond length changes after reduction and oxidation of $Ru(acac)_3$.

Property	$[Ru(acac)_3]^{-1}$	$[Ru(acac)_3]^{+1}$
Experimental Average Ru-O Bond Length Change [Å]	0.03 ± 0.01	-0.01 ± 0.01
Computed Average Ru-O Bond Length Change [Å]	0.043	-0.042

2.3. Charge Distribution During Reduction and Oxidation

The ligands on metal acetylacetonates are typically considered to be redox innocent, that is they do not contribute to the electrochemistry.[41] By tracking the oxidation state of Ru, we can determine the degree of innocence or non-innocence. One would expect the Ru oxidation states to change by ±1 if only the metal participated. The change in the charge on Ru following BE of $Ru(acac)_3$ was quantified by tracking edge shifts in the *in situ* XANES spectra (see Figure 5). The Ru edge shifts to lower energy during reduction and to higher energy during oxidation, and these shifts were reversible. For both reactions, the post-edge features did not change significantly. A shift of +1.25eV corresponds to a +1 change in the oxidation state of Ru (Figure 6a) based on the correlation of edge shifts for known standards

(results for the standard samples can be found in the Supplementary Information Figure S7). Given this correlation, the oxidation state of Ru decreases from 2.2±0.2 to 1.0±0.2 during the reduction of $Ru(acac)_3$ (Figure 6b). In other words, most of the electrochemistry is due to Ru. Also note that XANES spectra after reoxidizing the reduced $Ru(acac)_3$ (returning to zero electrons per molecule) were nearly identical to those for the fresh electrolyte.

Following electrochemical oxidation of $Ru(acac)_3$, the oxidation state of Ru increases from 2.2±0.2 to 2.9±0.2 or a net change of 0.7±0.2. The results indicate that while most of the electrochemistry can be attributed to the Ru, significant charge (~30±20%) is extracted from other constituents of the complex, namely the ligands. Given differences in products for the reduction and oxidation reactions, one might conclude that the stability of $Ru(acac)_3$ is correlated with the degree of charge that is stored on or extracted from Ru.

Experimentally determined changes in the oxidation states were compared to the quantified HOMO and LUMO densities determined from the DFT calculations (Table 3). A complete list of the orbital densities for each atom at each charge state for $Ru(acac)_3$ can be found in the Supplementary Information (Table S4). In all cases DFT calculations indicate less of the orbital density to be on the metal than determined from the XANES results; this is not unexpected as DFT is known to distribute charge throughout a complex.[36] Regardless, DFT predicts more of the orbital density to be on Ru during reduction of $Ru(acac)_3$ than during oxidation in agreement with the experimental results. The orbital densities for each atom type determined from the DFT calculations are shown in Figure 7. For the oxidized $Ru(acac)_3$ electrolyte, more of the orbital density is on the oxygen atoms than for the reduced $Ru(acac)_3$ electrolyte, and likewise for the carbon atoms, specifically those that are part of the conjugated ring portion of the acetylacetone ligands.

Both XANES and EXAFS of the oxidation reaction indicate the side reaction likely occurred on the conjugated portion of the ligands. K-edge XANES typically generate a pre-edge peak except when this is suppressed by inversion symmetry (e.g. octahedral) around the metal; this is a common method of quantifying transitions from octahedral (no pre-edge) to tetrahedral (strong pre-edge) in metals. In the case of Ru, a weak pre-edge shoulder is expected at 22,118 eV for non-inversion-symmetric species.[42] The lack of this feature in oxidized $Ru(acac)_3$ (Figure 5) indicates octahedral symmetry is maintained. Insights derived from results presented in this paper are being used to functionalize the acetylacetone to mitigate side reactions.

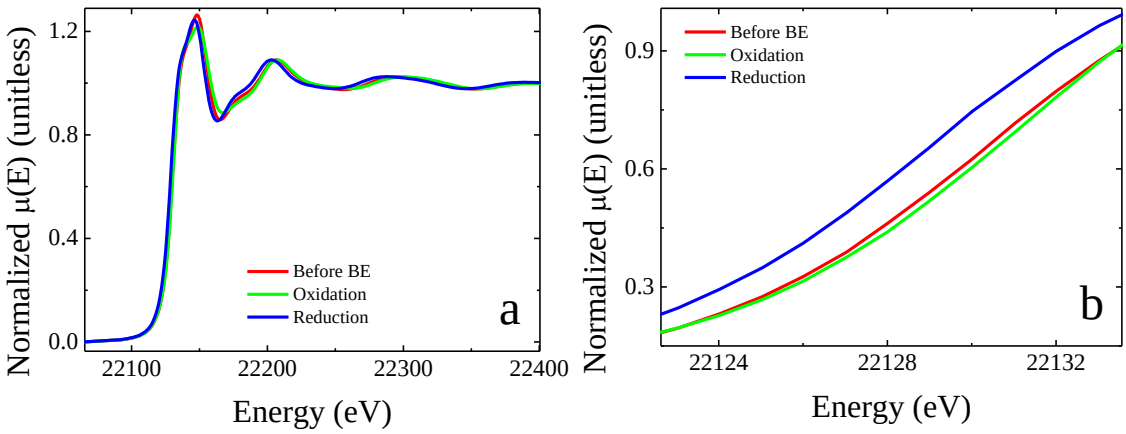

Figure 5. Full (a) and edge (b) XANES of $Ru(acac)_3$ solutions following reduction and oxidation via BE.

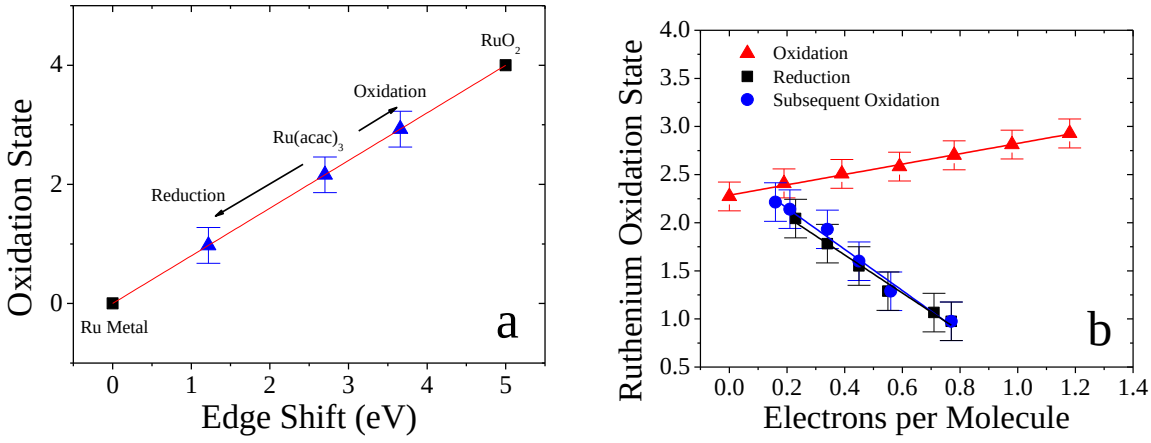

Figure 6. Edge shifts for standards and charged species associated with reduction and

oxidation reactions (determined from standards) (a) and XANES-estimated oxidation states of samples during reduction (black/blue) and oxidation (red) (b).

Table 3. Changes of oxidation state for Ru in $Ru(acac)_3$ during oxidation and reduction determined from XANES. The results are compared to the fraction of the orbital density as determined from DFT calculations.

Method	Reduction	Oxidation
XANES	-1.2±0.2	0.7±0.2
DFT	-0.67	0.53

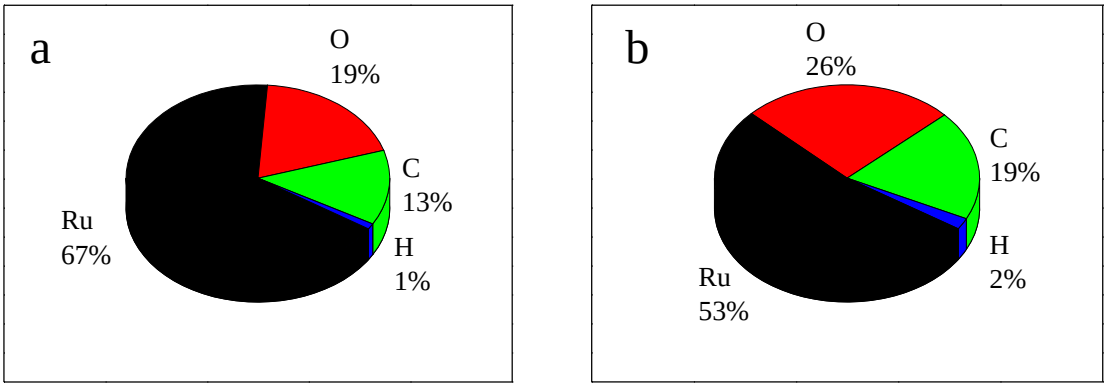

Figure 7. Neutral $Ru(acac)_3$ orbital density by atom type for LUMO (a) and HOMO (b).

3. Conclusions

The experimental and computational results presented in this paper indicate the reversible reduction of $Ru(acac)_3$ to $[Ru(acac)_3]^-$ in acetonitrile with essentially all of the charge localized to the metal center and the Ru-O bond length increasing on reduction and contracting during re-oxidation. The oxidation of $Ru(acac)_3$ in acetonitrile appeared to initially produce $[Ru(acac)_3]^+$ which converted to another species via chemical or electrochemical processes. Approximately 70% of the charge was extracted from the Ru atom and ~30% from the acetylacetone ligands. Collectively, the results suggest that while the short-term product of $Ru(acac)_3$ oxidation could be $[Ru(acac)_3]^+$, the long-term product has 6-fold Ru-O bonding with octahedral symmetry, has a structure that is identical to $Ru(acac)_3$ up to 3Å from Ru, has a Ru oxidation state of 2.9±0.2, and produced a couple at -0.2V vs Ag/Ag^+

which was found to be irreversible during BE. The results also indicate that stability and cyclability are functions of the degree of charge transfer with the metal center. Additional research will determine if this behavior is common to other metal acetylacetonates as well as other complexes.

4. Experimental Section

4.1. Cyclic Voltammetry

Cyclic voltammetry was performed using a PGSTAT302N Autolab Potentiostat. A 10 mL, three electrode electrochemical cell, fabricated in-house, was used for these experiments. The three electrodes consisted of a 0.07cm2 glassy carbon disk working electrode (BASi), a Ag/Ag+ quasi-reference electrode (BASi) filled with 0.01M silver tetrafluoroborate in acetonitrile (Sigma Aldrich), and a 23cm long platinum wire counter electrode (ALS). The working electrode was polished using 9 and 0.3μm aluminum oxide polishing paper (Fiber Instrument). Electrolyte solutions were prepared inside an Ar-filled VAC glove box, and all CV scans were conducted while inside the same glove box.

4.2. Bulk Electrolysis

Bulk electrolysis was performed using a PGSTAT100 Autolab Potentiostat with a chronoamperometric method. Holding potentials were chosen to isolate individual redox couples but avoid expected side reactions. A 10ml, glass cell consisting of two equal volume working and counter chambers separated by a class P5 (1.0-1.6μm pore size) glass frit (Adams&Chittenden) was fabricated in-house. The working electrodes were made from reticulated vitreous carbon sheets with 60 pores per inch (ERG Aerospace) that were cut into rectangular strips (~1x1x5cm^3). 0.07cm^2 glassy carbon working electrodes were used for in situ CV measurements which were polished using 9 and 0.3 μm aluminum oxide polishing paper (Fiber Instrument). A Ag/Ag^+ quasi-reference electrode (BASi) filled with 0.01M silver tetrafluoroborate in acetonitrile (Sigma Aldrich) was used as the reference electrode, and a

23cm long platinum wire (ALS) was used as the counter electrode. Two Teflon stir bars were used to mix the counter and working solutions during the experiments, and stirring was temporarily stopped during CV measurements. $Ru(acac)_3$, constant voltage BE was performed at a concentration of 0.1M active species with 0.5M $TBABF_4$ in acetonitrile. The same electrolyte was used in the counter chamber (equal volume as the working chamber). To characterize the oxidation reaction, the materials were evaluated following BE at 0.8 and 0.4V vs. Ag/Ag^+. To characterize the reduction reaction, the materials were evaluated following BE at -1.5 and -0.7V vs. Ag/Ag^+. A current cut-off of 1 mA was used for both reactions as cross-over occurs in the cell and a current lower than 1mA would not be reached. Samples before and after BE were diluted to 0.01M active species with 0.1M $TBABF_4$ in acetonitrile and CVs were collected.

4.3. X-ray absorption spectroscopy

The XAS experiments were performed at beamline 10-BM (MRCAT) of the Advanced Photon Source, Argonne National Laboratory. Beam size was set at 0.5 x 0.5mm and experiments were conducted in transmission mode with gas ionization chambers. XANES analysis consisted of observing changes in edge shift as well as transitions from one species to another as calculated by linear combination fitting (LCF) to known standards.

X-ray collection was taken from 200eV below the K edge of Ru metal (Ru K E_0 = 22117eV) to approximately 1200eV above the edge (~18$Å^{-1}$) with each measurement taken over the course of 30 minutes. EXAFS analysis was completed using the AUTOBK algorithm with a spline range from 0 to 18$Å^{-1}$, Rbkg=1.0 and a normalization order of 3. The EXAFS range was found to be excellent out to 18$Å^{-1}$ and a Fourier transform was made using 3<k<16A^{-1}. Measurement of Ru standards of Ru metal, $Ru(acac)_3$, tris(triphenylphosphine) ruthenium (II) dichloride (TTP-$RuCl_2$), RuO_2, $RuCl_3$ were taken in polycarbonate cuvettes (liquid samples) or ground to a fine powder and loaded into polyimide tape packets (solid samples).

A BE cell described in section 4.5 was placed in the beamline such that a 1cm length of electrolyte could be measured in transmission mode (edge step ~0.7). The negative and positive reactions were tested separately by conducting BE of the individual half-reactions charged from 0% ("before electrolysis") to the maximum electrons per molecule in steps of 0.2, and subsequent discharge, with XAS measurement taken at each step. The BE experiment was conducted using the same method as described in section 4.2 while using the Teflon cell. For the reduction reaction, the electrons per molecule were determined using the open circuit potential and the Nernst equation. For the oxidation reaction, the open circuit potential was not a reliable method of determining the electrons per molecule due to the side reaction changing the open circuit potential. Monitoring of current during each step demonstrated negligible changes in the oxidation state of the electrolyte while XAS was being collected.

4.4. Density Function Theory Calculations

Structure optimization calculations were performed for the neutral and charged species using the B3LYP functional with the 6-31+G(d) and LANL2DZ basis sets. All minimized structures were confirmed by vibrational frequency calculations. The B3LYP functional with 6-31+G(d) basis set has been previously shown to be effective at determining the standard potentials of both ionic liquids and quinoxaline derived complexes,[43,44] and similar DFT calculations have been shown to correctly predict the reduction standard potentials of various metal-acetylacetonate complexes. In previous metal-acetylacetonate studies, no oxidation potentials, structural changes during charge/discharge, or charge states were presented.[45] The LANL2DZ basis set has been used for complexes similar to $Ru(acac)_3$ to effectively determine the charge of the metal vs. ligand for neutral species using Natural Population Analysis (NPA), and calculating molecular orbital energies.[46] First, the predicted standard potentials were calculated using the highest occupied molecular orbitals (HOMO) and lowest unoccupied molecular orbitals (LUMO) values of the neutral species in acetonitrile using the

Polarizable Continuum Model (PCM). A linear correlation found by Cheng and colleagues for 295 organic complexes[43] was used to convert the calculated HOMO and LUMO energies to the positive and negative standard potentials respectively. The optimized structures with different charges were compared to determine any significant changes in bond lengths and angles to compare with the XAS results.

To quantify the HOMO and LUMO density for the complex, Multiwfn, a multifunctional wavefunction analyzer developed by Beijing Kein Research Center for Natural Sciences was utilized, using the Hirshfeld method.[37]

4.5. Cell Design

A custom Teflon cell was built for use in the *in situ* X-ray absorption experiments run at Argonne National Lab, constructed in the Physics machine shop at the University of Michigan. The cell consisted of three parts: a working electrode chamber, a counter electrode chamber, and a block used to seal a P5 glass frit (Adams & Chittenden) between the two electrode chambers. The dimensions of the counter and working electrode cavities were designed to ensure that the liquid heights were equal when using 5mL of solution in both chambers. The counter electrode chamber (shown on the left side of all explosion diagrams in Figure 8 consists of a 2" long cavity of 0.625" diameter. At the top of the cavity was threading for a 1/2" NPT fitting, where a Pt wire counter electrode was secured using a ¼" Swagelok ultra-torr fitting. A 0.9cm diameter hole was cut into the cavity with an expanded diameter (to 1cm diameter) at the edge to house a #12 viton o-ring. In the middle, connecting block, a 1cm diameter hole is cut 8mm into the 1cm slab, with the last 2mm consisting of a reduced hole of 0.9cm diameter to house a #12 viton o-ring. The working electrode chamber (Figure 9) consisted of a large rectangular cavity to house the working and reference electrodes, and a 1cm x 1cm x 1cm cavity, which acted as the viewing area for X-rays. 7.5mm diameter holes were cut into the sides of the 1x1x1cm cavity, leaving ~250μm thick walls of Teflon to act as

"windows" for the X-rays while maintaining an air-tight seal. The working electrode chamber was sealed against the connecting block using a #26 Viton o-ring, housed in an o-ring cut-out. The working electrode, a 1x1x5cm^3 strip of 60 pore per inch reticulated vitreous carbon (ERG Aerospace*)* attached to a wire using silver epoxy and a 7mm glass tube, was secured in the top of the working electrode chamber using a 1/4" Swagelok ultra-torr fitting with an 1/8" NPT outlet. The reference electrode (Ag/Ag^+) was similarly secured using a 1/4" ultra-torr to 1/8" NPT Swagelok fitting at a 30° angle to the bottom face, aimed at contacting the top of the liquid in the cell. Prior to the experiments at Argonne National Lab, the cell was validated at UM by performing bulk electrolysis on a 0.1M $Ru(acac)_3$ with 0.5M $TBABF_4$ in acetonitrile solution, with similar results obtained in the glass BE cell. Further, cyclic voltammograms were obtained to ensure no peaks associated with water or unknown products were found following air exposure to the Teflon cell for 12 hours, well in excess of the time required for the bulk electrolysis experiments.

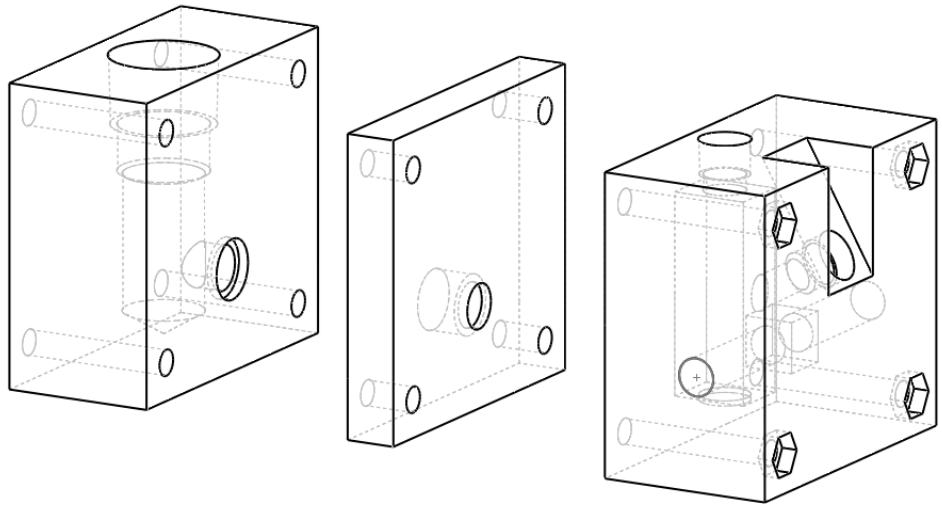

Figure 8. Explosion diagrams of the bulk electrolysis cell used in the in situ X-ray absorption experiments. From left to right: Counter electrode block, connected block, working electrode block.

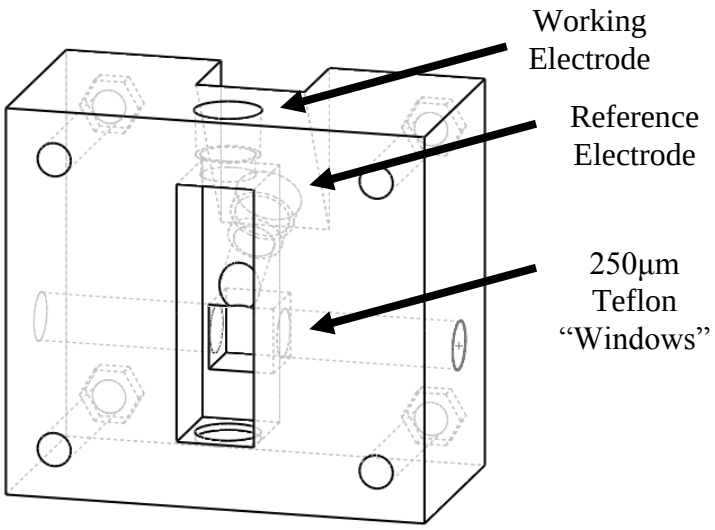

Figure 9. Schematic of working electrode chamber.

Figure 10. Assembled Bulk Electrolysis cell.

Supporting Information

Supporting Information is available from the Wiley Online Library or from the author.

Acknowledgements

Research described in this paper was supported primarily by a grant from the National Science Foundation, Sustainable Energy Pathways Program (NSF-1230236). Partial support was also provided by the U.S. Department of Energy through the Joint Center for Energy Storage Research (JCESR). MRCAT operations are supported by the Department of Energy and the MRCAT member institutions. This research used resources of the Advanced Photon Source, a U.S. Department of Energy (DOE) Office of Science User Facility operated for the DOE Office of Science by Argonne National Laboratory under Contract No. DE-AC02-06CH11357. The authors also thank the University of Michigan Physics Machine Shop for suggestions regarding the cell design and for meeting an aggressive timeline.

Received: ((will be filled in by the editorial staff))

Revised: ((will be filled in by the editorial staff))

Published online: ((will be filled in by the editorial staff))

[1] A. Z. Weber, M. M. Mench, J. P. Meyers, P. N. Ross, J. T. Gostick, Q. Liu, *J. Appl. Electrochem.* **2011**, *41*, 1137.

[2] P. Denholm, E. Ela, B. Kirby, M. Milligan, *Contract* **2010**, *NREL*, 1.

[3] L. Jorrissen, H. Frey, *Encycl. Electrochem. Power Sources* **2009**, 215.

[4] U.S. Department of Energy, Grid Energy Storage, **2013**, 33.

[5] W. Wang, Q. Luo, B. Li, X. Wei, L. Li, Z. Yang, *Adv. Funct. Mater.* **2013**, *23*, 970.

[6] A. J. Bard, L. R. Faulkner, *Electrochemical Methods: Fundamentals and Applications*, **2001**.

[7] R. M. Darling, K. G. Gallagher, F. R. Brushett, **2014**, *7*, 3459.

[8] P. J. Cappillino, H. D. Pratt, N. S. Hudak, N. C. Tomson, T. M. Anderson, M. R. Anstey, *Adv. Energy Mater.* **2014**, *4*.

[9] Y. Huang, S. Gu, Y. Yan, S. F. Y. Li, *Curr. Opin. Chem. Eng.* **2015**, *8*, 105.

[10] P. J. Cabrera, X. Yang, J. A. Suttil, K. L. Hawthorne, R. E. M. Brooner, M. S. Sanford, L. T. Thompson, *J. Phys. Chem. C* **2015**, *119*, 15882.

[11] S.-H. Shin, S.-H. Yun, S.-H. Moon, *RSC Adv.* **2013**, *3*, 9095.

[12] D. Zhang, H. Lan, Y. Li, *J. Power Sources* **2012**, *217*, 199.

[13] H. D. Pratt, N. S. Hudak, X. Fang, T. M. Anderson, *J. Power Sources* **2013**, *236*, 259.

[14] Y. Matsuda, K. Tanaka, M. Okada, Y. Takasu, M. Morita, T. Matsumura-Inoue, *J. Appl. Electrochem.* **1988**, *18*, 909.

[15] T. Yamamura, Y. Shiokawa, H. Yamana, H. Moriyama, *Electrochim. Acta* **2002**, *48*, 43.

[16] L. Cosimbescu, X. Wei, M. Vijayakumar, W. Xu, M. L. Helm, S. D. Burton, C. M. Sorensen, J. Liu, V. Sprenkle, W. Wang, *Sci. Rep.* **2015**, *5*, 14117.

[17] I. L. Escalante-Garcia, J. S. Wainright, L. T. Thompson, R. F. Savinell, *J. Electrochem. Soc.* **2014**, *162*, A363.

[18] T. Herr, P. Fischer, J. Tübke, K. Pinkwart, P. Elsner, *J. Power Sources* **2014**, *265*, 317.

[19] T. Herr, J. Noack, P. Fischer, J. Tübke, *Electrochim. Acta* **2013**, *113*, 127.

[20] Q. Liu, A. a. Shinkle, Y. Li, C. W. Monroe, L. T. Thompson, A. E. S. Sleightholme, *J. Power Sources* **2011**, *196*, 5742.

[21] A. a. Shinkle, A. E. S. Sleightholme, L. D. Griffith, L. T. Thompson, C. W. Monroe, *J. Power Sources* **2012**, *206*, 490.

[22] A. E. S. Sleightholme, A. a. Shinkle, Q. Liu, Y. Li, C. W. Monroe, L. T. Thompson, *J.*

Power Sources **2011**, *196*, 5742.

[23] A. a. Shinkle, A. E. S. Sleightholme, L. T. Thompson, C. W. Monroe, *J. Appl. Electrochem.* **2011**, *41*, 1191.

[24] Q. Liu, A. E. S. Sleightholme, A. a. Shinkle, Y. Li, L. T. Thompson, *Electrochem. commun.* **2009**, *11*, 2312.

[25] A. a. Shinkle, T. J. Pomaville, A. E. S. Sleightholme, L. T. Thompson, C. W. Monroe, *J. Power Sources* **2014**, *248*, 1299.

[26] J. A. Suttil, J. F. Kucharyson, I. L. Escalante-Garcia, P. J. Cabrera, B. R. James, P. R. F. Savinell, M. S. Sanford, L. Thompson, *J. Mater. Chem. A* **2015**, *00*, 1.

[27] M. H. Chakrabarti, R. a W. Dryfe, E. P. L. Roberts, *Electrochim. Acta* **2007**, *52*, 2189.

[28] J. Mun, M.-J. Lee, J.-W. Park, D.-J. Oh, D.-Y. Lee, S.-G. Doo, *Electrochem. Solid-State Lett.* **2012**, *15*, A80.

[29] W. Wang, W. Xu, L. Cosimbescu, D. Choi, L. Li, Z. Yang, *Chem. Commun.* **2012**, *48*, 6669.

[30] X. Wei, W. Xu, M. Vijayakumar, L. Cosimbescu, T. Liu, V. Sprenkle, W. Wang, *Adv. Mater.* **2014**, *26*, 7649.

[31] B. Huskinson, M. P. Marshak, C. Suh, S. Er, M. R. Gerhardt, C. J. Galvin, X. Chen, A. Aspuru-Guzik, R. G. Gordon, M. J. Aziz, *Nature* **2014**, *505*, 195.

[32] J. Huang, L. Su, J. a. Kowalski, J. L. Barton, M. Ferrandon, A. K. Burrell, F. R. Brushett, L. Zhang, *J. Mater. Chem. A* **2015**, *3*, 14971.

[33] G. Nagarjuna, J. Hui, K. J. Cheng, T. Lichtenstein, M. Shen, J. S. Moore, J. Rodriguez-Lopez, **2014**, *136*, 16309.

[34] X. Wei, L. Cosimbescu, W. Xu, J. Z. Hu, M. Vijayakumar, J. Feng, M. Y. Hu, X. Deng, J. Xiao, J. Liu, V. Sprenkle, W. Wang, *Adv. Energy Mater.* **2014**, 1.

[35] C. a. Apblett, D. M. Stewart, R. T. Fryer, J. C. Sell, H. D. I. Pratt, T. M. Anderson, R. W. Meulenberg, *Electrochim. Acta* **2015**, *185*, 156.

[36] Gaussian 09, Revision E.01, M. J. Frisch, G. W. Trucks, H. B. Schlegel, G. E. Scuseria, M. A. Robb, J. R. Cheeseman, G. Scalmani, V. Barone, B. Mennucci, G. A. Petersson, H. Nakatsuji, M. Caricato, X. Li, H. P. Hratchian, A. F. Izmaylov, J. Bloino, G. Zheng, J. L. Sonnenberg, M. Hada, M. Ehara, K. Toyota, R. Fukuda, J. Hasegawa, M. Ishida, T. Nakajima, Y. Honda, O. Kitao, H. Nakai, T. Vreven, J. Montgomery, J. A., J. E. Peralta, F. Ogliaro, M. Bearpark, J. J. Heyd, E. Brothers, K. N. Kudin, V. N. Staroverov, R. Kobayashi, J. Normand, K. Raghavachari, A. Rendell, J. C. Burant, S. S. Iyengar, J. Tomasi, M. Cossi, N. Rega, J. M. Millam, M. Klene, J. E. Knox, J. B. Cross, V. Bakken, C. Adamo, J. Jaramillo, R. Gomperts, R. E. Stratmann, O. Yazyev, A. J. Austin, R. Cammi, C. Pomelli, J. W. Ochterski, R. L. Martin, K. Morokuma, V. G. Zakrzewski, G. A. Voth, P. Salvador, J. J. Dannenberg, S. Dapprich, A. D. Daniels, Ö. Farkas, J. B. Foresman, J. V. Ortiz, J. Cioslowski, D. J. Fox, **2009**.

[37] N. M. O'Boyle, A. L. Tenderholt, K. M. Langner, *J. Comput. Chem.* **2008**, *29*, 839.

[38] M. A. Nawi, T. L. Riechel, *Inorg. Chem.* **1981**, *20*, 1974.

[39] H. Ikeuchi, K. Naganuma, M. Ichikawa, H. Ozawa, T. Ino, M. Sato, H. Yonezawa, S. Mukaida, A. Yamamoto, T. Hashimoto, *J. Solution Chem.* **2007**, *36*, 1243.

[40] S. Kar, N. Chanda, S. M. Mobin, A. Datta, F. A. Urbanos, V. G. Puranik, R. Jimenez-aparicio, G. K. Lahiri, *Inorg. Chem.* **2004**, *43*, 4911.

[41] Z. Zhang, S. S. Zhang, Eds. , *Rechargeable Batteries: Materials, Technologies and*

New Trends, Springer International Publishing, **2015**.

[42] K. Getty, M. U. Delgado-Jaime, P. Kennepohl, *Inorganica Chim. Acta* **2008**, *361*, 1059.

[43] L. Cheng, R. S. Assary, X. Qu, A. Jain, S. P. Ong, N. N. Rajput, K. Persson, L. A. Curtiss, *J. Phys. Chem. Lett.* **2015**, *6*, 283.

[44] N. Shao, X. Sun, S. Dai, D. Jiang, *J. Phys. Chem. B* **2011**, 12120.

[45] R. Freitag, COMPUTATIONAL, STRUCTURAL AND ELECTROCHEMICAL PROPERTIES OF METAL(III)Tris-BETADIKETONATO COMPLEXES, University of the Free State, Dissertation, **2013**.

[46] D. Kalinina, C. Dares, H. Kaluarachchi, P. G. Potvin, A. B. P. Lever, *Inorg. Chem.* **2008**, *47*, 10110.